Unexpected Three-State Hydrochromism of a Donor-Acceptor Self-Complex with Fluctuations in Relative Humidity

Zhimin Sun,[a] Zhenzhen Wang,[b] Yanhai Ni, [a] Lihui Xi,[a] Loïc M. Roch,[a] Hany F. Nour,[c] and Mark A. Olson[*,a, d]

[a]*School of Pharmaceutical Science and Technology, Tianjin University, Tianjin, China*
[b]*Academy of Chinese Medical Science, Henan University of Chinese Medicine, Zhengzhou, China*
[c]*Photochemistry Department, National Research Centre, Cairo, Egypt*
[d]*Department of Chemistry, Northwestern University, Evanston, IL. USA*

Electronic Supporting Information

Table of Contents

1. Materials and General Methods

Starting materials, reagents, and solvents were purchased as reagent grade and used without further purification. **2**·1Br was synthesized as previously reported[1] All reactions were performed under an argon atmosphere and in dry solvents unless otherwise noted. Analytical thin-layer chromatography (TLC) was performed on aluminum sheets, percolated with silica gel GF254, visualized by exposure to ultraviolet light. Deuterated solvents (Cambridge Isotope Laboratories) for NMR spectroscopic analyses were used as received. ^{1}H and ^{13}C NMR spectra were recorded on a Bruker Advance III 400 MHz spectrometer.Chemical shifts values are given in ppm and calibrated relative to the residual signal of the solvent. The peak patterns are defined as follows: s, singlet; d, doublet; t, triplet; q, quartet; qui, quintet; m, multiplet; dd, doublet of doublets, and td, triplet of doublets. The coupling constants J, are reported in Hertz (Hz). Flash column chromatography was performed over silica gel (260−400 mesh or 300−400 mesh) using a mixture of n-hexane and ethyl acetate (EtOAc) or methanol and NH_4Cl (2M) aqueous as the eluent. TLC plates (Silica gel GF254) were visualized by exposure to ultraviolet light. High-resolution mass spectrometry (HRMS) was obtained on a Q-TOF micro spectrometer using electrospray ionization (ESI) technique in either positive mode or negative mode. Compound melting points and thermochromic transition temperatures for the xerogel films were recorded on a RY-1 Melting point apparatus equipped with a magnified viewing window with internal light and a digital temperature probe. UV-Vis and reflectance spectra were recorded on both a HITACHI U-3900 and an Ocean Optics fiber-optic spectrophotometer. Powder X-ray diffraction was conducted on a Rigaku D/MAX 2500 X-ray diffractometer using Cu-Kα radiation (λ = 1.54178 Å). The voltage and the current were 40 kV and 100 mA, respectively. Samples were measured in reflection mode in the 2θ range of 2–40° with a scan speed of 8° min^{-1}. Data were acquired at ambient temperature (20 °C). Thermogravimetric analysis was conducted in a Mettler TGA/ DSC 1 STAR^{e} System, using a nitrogen gas purge flow of 20 mL min^{-1} and a scan rate of 10 °C min^{-1}. Dynamic vapor sorption experiments were performed using a TA

Instrument's VTI-SA+ DVS.

2. Synthetic Procedures and Spectroscopic Characterization

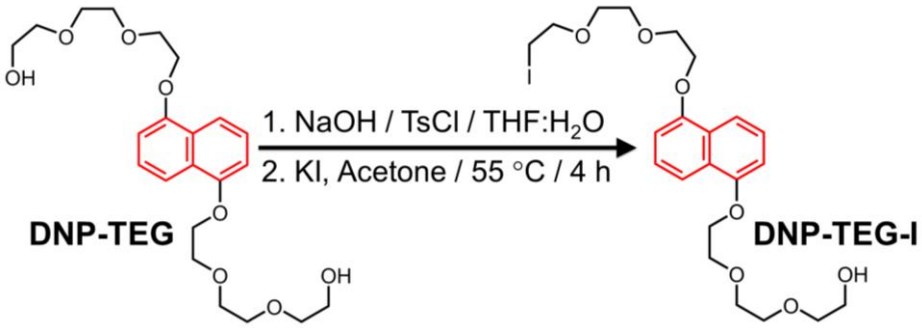

DNP-TEG-I: NaOH (2.64 g, 66 mmol in 20 mL of water) was added to a solution of **DNP-TEG** (14 g, 33 mmol) in THF (60 ml). The mixture was stirred at 0 ℃ for 0.5 h, then a solution of TsCl (8.2 g, 43 mmol) in THF was added dropwise to the mixture. The reaction mixture was stirred for 2 hrs, and then the THF was removed under vacuum. Water was added to the crude product and extracted with CH_2Cl_2 three times. The combined organic phases were dried with Na_2SO_4 and the solvent was removed under vacuum. The residue was purified by column chromatography on silica gel (200−300 mesh) using gradient EtOAc/n-hexane (from 1:3 to 3:1) as the eluent to provide a solid (15.6 g). Then the solid was dissolved in acetone. NaI (5.4 g, 36 mmol) was added to the solution and the reaction mixture was heated at 55 °C for 4 hrs. The reaction mixture was then cooled to r.t. and the solvent was removed under vacuum. Water was added to the crude product and extracted with CH_2Cl_2 three times. The combined organic phases were dried with Na_2SO_4 and the solvent was removed under vacuum to provide desired product as a white solid (12.6 g, 40%). **DNP-TEG-I**: Mp：40-42 ^oC. ^1H NMR ($CDCl_3$, 400 MHz, 25 ^oC): δ = 2.51 (s, 1H), 3.24 (t, J = 6.9 Hz, 2H), 3.57–3.63 (m, 2H), 3.66–3.83 (m, 12H), 3.96–4.01 (m, 4H), 4.29 (t, J = 4.8 Hz, 4H), 6.83 (d, J = 7.7 Hz, 2H), 7.35 (t, J = 8.0 Hz, 2H), 7.86 (d, J = 8.5 Hz, 2H); ^{13}C NMR ($CDCl_3$, 100 MHz, 25 ^oC): 3.2, 61.9, 68.0, 68.1, 69.97, 70.04, 70.5, 70.6, 71.1, 71.2, 72.2, 72.7, 105.9, 114.7, 114.8, 125.25, 125.26, 126.91, 126.93, 154.4, 154.5. HRMS (ESI): m/z calcd for $C_{22}H_{31}IO_7$: 557.1007; found: 557.1005 $[M + Na]^+$.

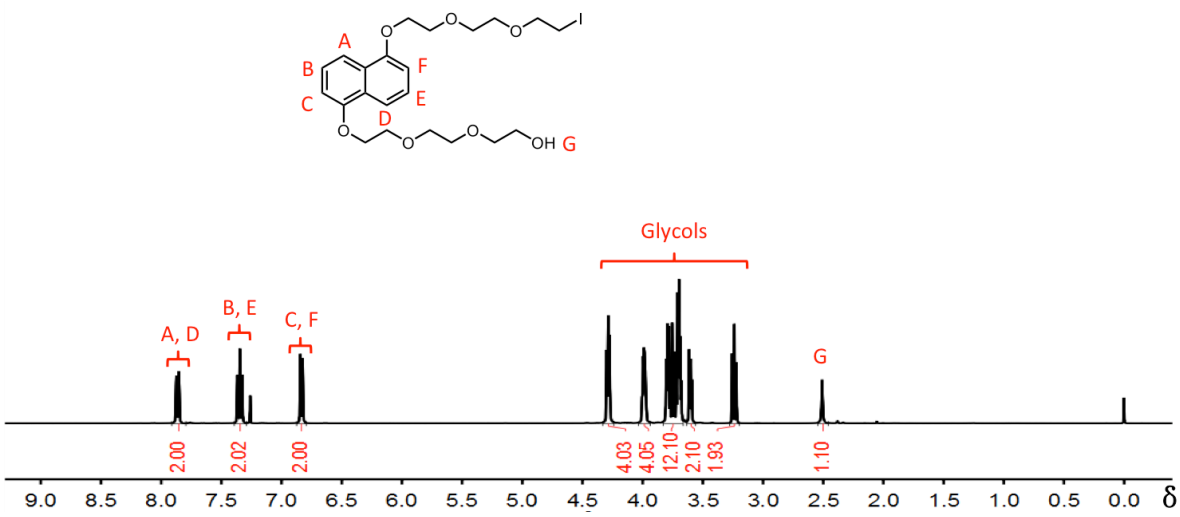

Figure S1: ^{1}H NMR spectrum of DNP-TEG-I in CDCl3 at 298 K (400 MHz)

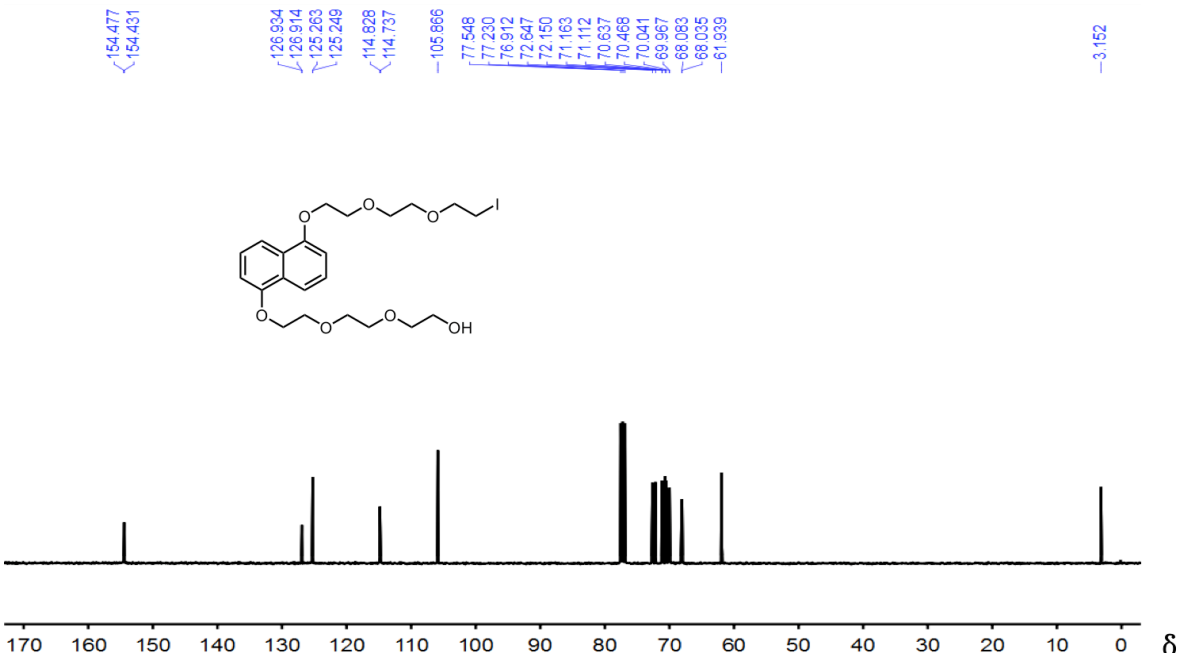

Figure S2: ^{13}C NMR spectrum of DNP-TEG-I in CDCl3 at 298 K (100 MHz)

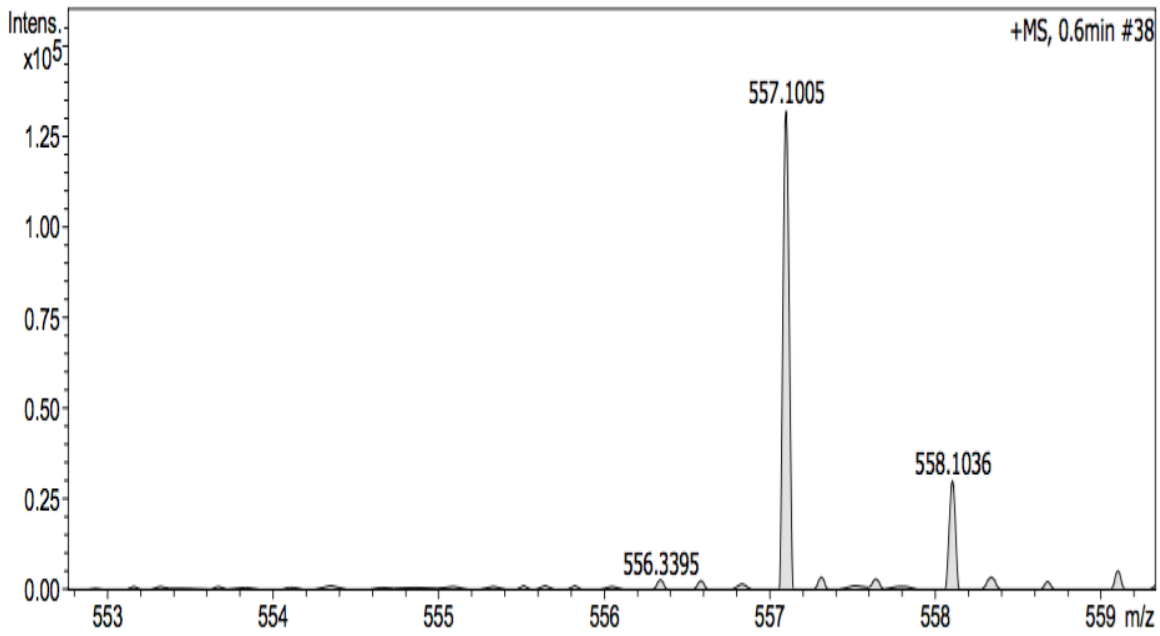

Figure S3: Mass spectrum of DNP-TEG-I

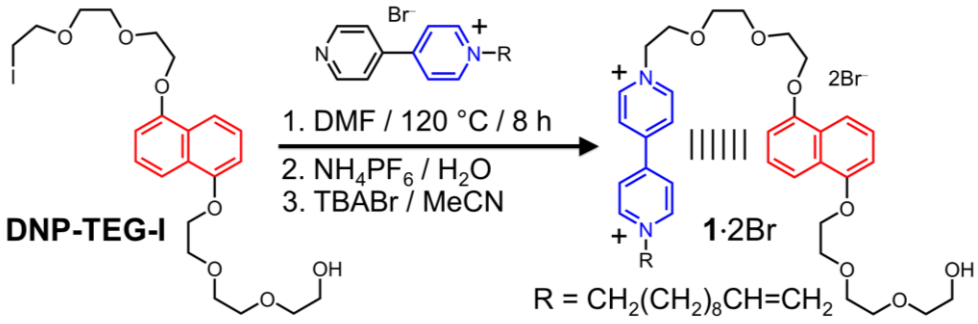

1·2Br: **2**·1Br (1.47 g, 3.75 mmol) and **DNP-TEG-I** (4.5 g, 8.42 mmol) were combined in anhydrous DMF (5 ml) and heated at 120 °C for 8 hrs. The reaction mixture was then cooled to r.t. and the solvent was removed under vacuum. The residue was purified by column chromatography on silica gel (300−400 mesh) using a gradient of methanol/ 2M NH_4Cl solution in H_2O (from 10:1 to 1:1) as the eluent. The eluent solutions containing the product were concentrated under vacuum and then redissolved in H_2O. Saturated aqueous NH_4PF_6 was added dropwise until no further precipitate formed. *Counter-ion exchange to dibromide salts*: The precipitate was filtered and washed three times with excess water and then redissolved in acetone (50 ml). A saturated solution of tetrabutylammonium bromide (TBAB)

in acetone was added dropwise until no further precipitate formed. The precipitate was then filtered and washed using acetone for three times under the protection of argon to afford the dibromide salt, **1**·2Br as a yellow, red, or purple solid depending on RH (1.4 g, 43%). **1**·2Br: Mp: Decomposes at 190 °C. ^{1}H NMR (D_2O, 400 MHz, 25 ^{o}C, 5 mM): δ = 1.18–1.41 (m, 24H), 1.93–2.05 (m, 8H), 3.86 (s, 8H), 3.93–3.98 (m, 4H), 4.10–4.19 (m, 4H), 4.20–4.30 (m, 4H), 4.55 (t, J = 7.3 Hz, 4H), 4.85–5.06 (m, 8H), 5.86 (ddt, J = 6.7, 10.3, 17.0 Hz, 2H), 6.90 (d, J = 7.7 Hz, 2H), 7.02 (d, J = 8.4 Hz, 2H), 7.23 (t, J = 8.0 Hz, 2H), 7.84 (d, J = 6.6 Hz, 4H), 8.06 (d, J = 6.8 Hz, 4H), 8.69 (d, J = 6.7 Hz, 4H), 9.02 (d, J = 6.9 Hz, 4H); ^{13}C NMR (D_2O, 100 MHz, 25 ^{o}C, 30 mM): δ = 25.5, 28.3, 28.6, 28.78, 28.83, 30.9, 33.3, 61.2, 62.0, 67.8, 68.5, 69.6, 69.9, 70.4, 106.3, 113.5, 114.1, 125.4, 125.9, 126.0, 126.3, 139.2, 145.0, 146.0, 148.0, 148.3, 153.5; HRMS (ESI): m/z calcd for $C_{43}H_{60}N_2O_7Br_2$: 358.2195; found: 358.2190 $[M - 2Br]^{2+}$. **1**·2Cl: Mp: Decomposes at 210 °C. ^{1}H NMR (D_2O, 400 MHz, 25 ^{o}C, 5 mM): δ = 1.20–1.49 (m, 12H), 1.94–2.13 (m, 4H), 3.59–3.64 (m, 2H), 3.65–3.70 (m, 2H), 3.71–3.77 (m, 4H), 3.85 (s, 6H), 3.94 (s, 2H), 4.05 (s, 2H), 4.17 (s, 4H), 4.38 (s, 2H), 4.61 (t, J = 7.2 Hz, 2H), 4.87–5.03 (m, 4H), 5.85 (ddt, J = 6.5, 10.2, 16.7 Hz, 1H), 6.89 (d, J = 7.6 Hz, 1H), 6.99 (d, J = 7.5 Hz, 1H), 7.29 (dt, J = 8.1, 13.4 Hz, 3H), 7.43 (d, J = 6.8 Hz, 1H), 7.85 (d, J = 6.4 Hz, 2H), 8.05 (d, J = 6.6 Hz, 2H), 8.73 (d, J = 6.4 Hz, 2H), 9.04 (d, J = 6.6 Hz, 2H).

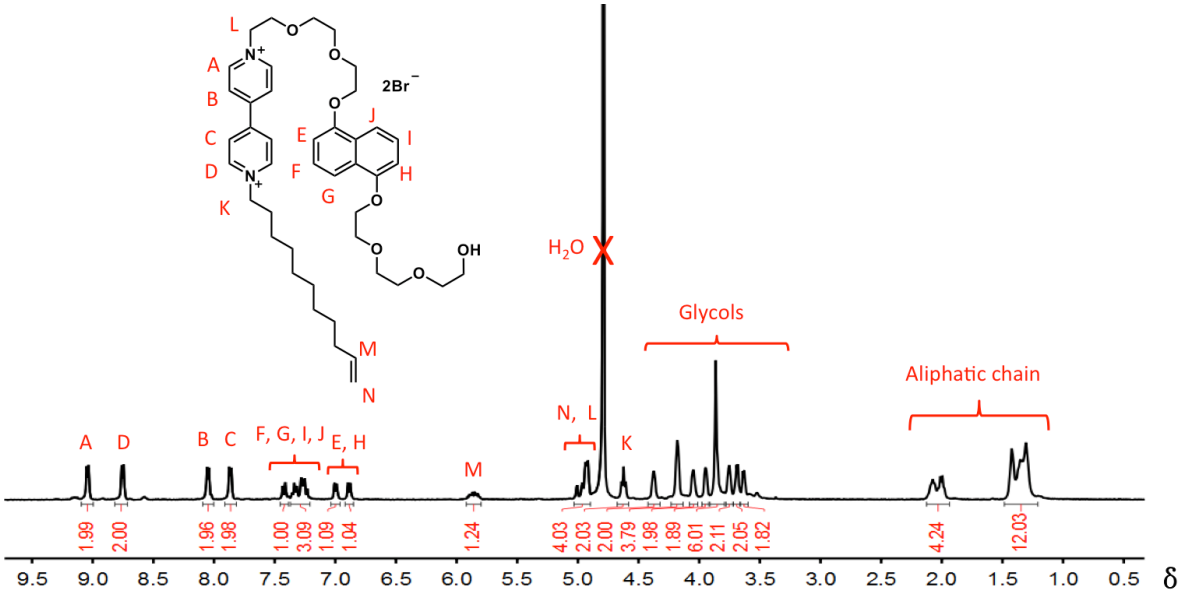

Figure S4: ^{1}H NMR spectrum of 5 mM solution of 1·2Br in D2O at 298 K (400 MHz)

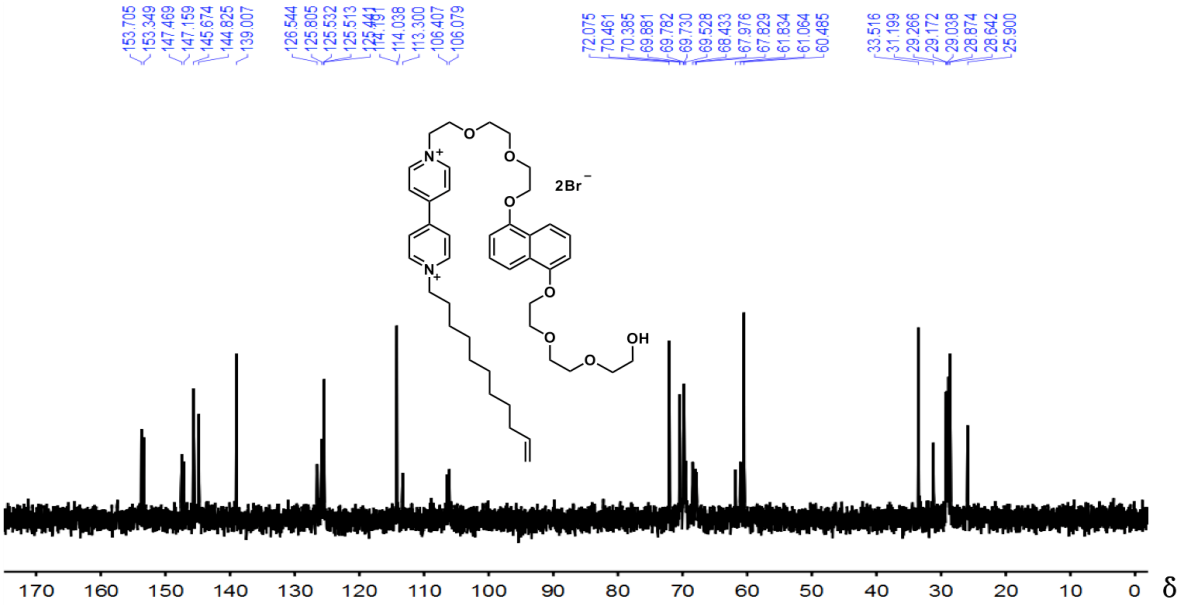

Figure S5: ^{13}C NMR spectrum of 30 mM solution of 1·2Br in D2O at 298 K (100 MHz)

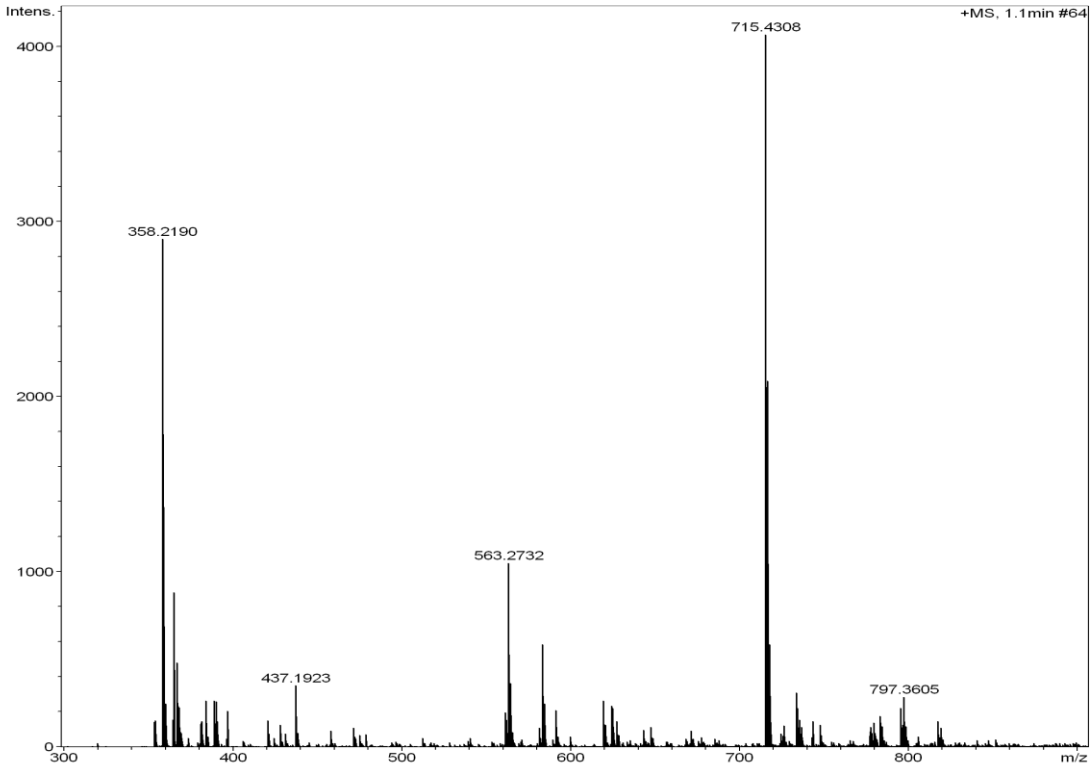

Figure S6: Mass spectrum of 1·2Br

3. Film Sample Preparation and Humidity Treatment

Sealed humidity chambers were constructed from an airtight commercial 30×30×30 cm clear plastic cubic cabinet. A beaker with a diameter 7.5 cm and a height of 7.5 cm was filled with 100 ml of a saturated salt solution and placed into the humidity chamber. Depending on the desired relative humidity, saturated aqueous solutions of KOAc, K_2CO_3, NaBr, NaCl, and KCl were used to maintain a relative humidity's of 32, 40, 58, 70, and 81% respectively. The average relative humidity within the chamber was monitored electronically using a DT-625 humidity sensor.

A solution of **1**·2Br (150 mM) in methanol was prepared and drop casted onto a standard 7.6 cm × 2.6 cm glass microscope slide. Gentle heating was applied to the glass slide by way of hot plate to slowly remove the solvent until smooth films were obtained. In order to obtain solvated (red) xerogel films of **1**·2Br, the xerogel films were placed in a sealed humidity chamber maintained at 70 % relative humidity for 12 hours. In order to obtain the films of the **1**·2Br hydrate (purple), solvated (red) films were removed from the 70 % relative humidity chamber and placed in a sealed humidity chamber for 12 hours maintained at 32 % relative humidity during which time the red solvated film sample of **1**·2Br underwent a pronounced red to purple color transition. In order to obtain films of the **1**·2Br anhydrate (yellow), purple hydrate samples of **1**·2Br were heated to over 125 °C in order to liberate coordinating waters. Upon removal of coordinating waters, the purple hydrate sample of **1**·2Br underwent a pronounced purple to yellow color transition. Samples prepared in this manner were then employed as is or scraped off the glass slide for further characterization. Stamped ink prints were prepared from an aqueous 200 mM stock solution of **1**·2Br using standard commercial rubber stamps.

For the measurement of time dependent and variable humidity UV-Vis absorption spectra, a humidity chamber equipped with a dual gas/liquid mass flow controller was employed to regulate and maintain a constant humidity from 0 to 100 % relative humidity using dry Ar gas and syringe pump. Spectra was collected using a fiber optic spectrometer in-situ and the average relative humidity during these experiments was monitored electronically using a

DT-625 humidity sensor.

The stability of the anhydrate (yellow), hydrate (purple), and solvated (red) films of **1**·2Br to various humidity conditions was determined by subjecting each sample to humidity conditions ranging from 5.4 to 81 % relative humidity while monitoring for an observable color change (Table S1

Table S1: Film Hydration State Stability Testing at Various Humidities

Humidity (%)	Anhydrate **1**·2Br	Solvated **1**·2Br	Hydrate **1**·2Br
5.4[a]	Yellow	Yellow	Purple
8.8[a]	Yellow	Yellow	Purple
13[a]	Yellow	Yellow	Purple
21[a]	Yellow	Yellow	Purple
32[b]	Yellow	Purple	Purple
40[c]	Yellow	Purple	Purple
58[d]	Yellow	Purple	Purple
70[e]	Red	Red	Red
81[f]	Red	Red	Red

[a]Sample exposed to laboratory humidity conditions outside of the humidity chamber. [b]Humidity chamber conditions maintained using a saturated aqueous solution of KOAc. [c]Humidity chamber conditions maintained using a saturated aqueous solution of K_2CO_3. [d]Humidity chamber conditions maintained using a saturated aqueous solution of NaBr. [e]Humidity chamber conditions maintained using a saturated aqueous solution of NaCl. [f]Humidity chamber conditions maintained using a saturated aqueous solution of KCl.

4. UV/Vis Absorption Spectroscopy

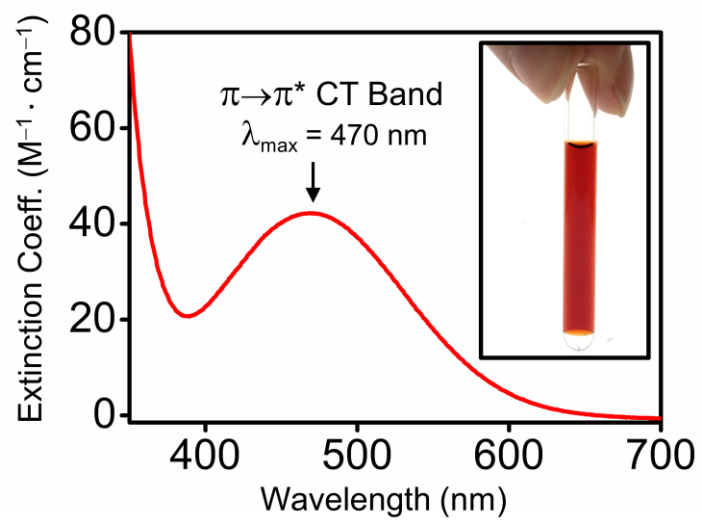

Figure S7: UV-Vis absorption spectrum of a 2.5 × 10^{-2} M aqueous solution of **1**·2Br measured across a .5 cm path length cuvette and (inset) a photograph of an aqueous solution of **1**·2Br.

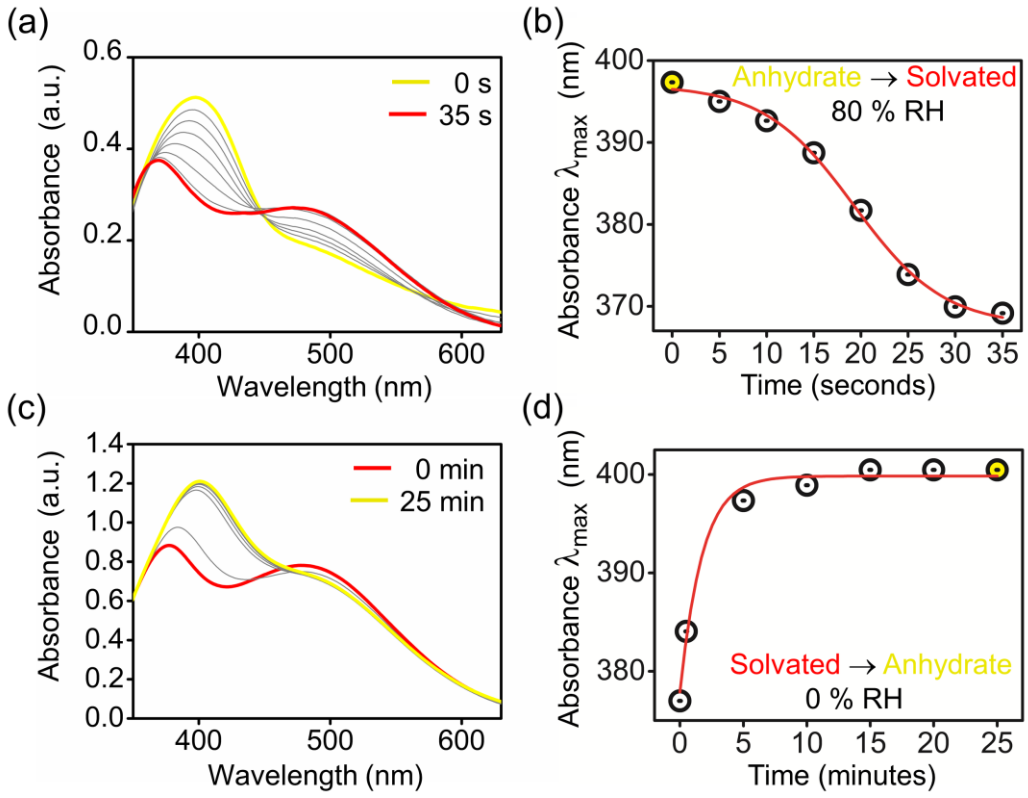

Figure S8: Overlaid absorption spectra and absorption lambda max values (λ_{max}) of a dropcast film of **1**·2Br measured at different time intervals during the conversion of the (a-b) anhydrate state (yellow trace) to the solvated state (red trace) within an humidity chamber maintained at 80% relative humidity and during the conversion of the (c-d) solvated state to the anhydrate state within a humidity chamber maintained at 0% relative humidity.

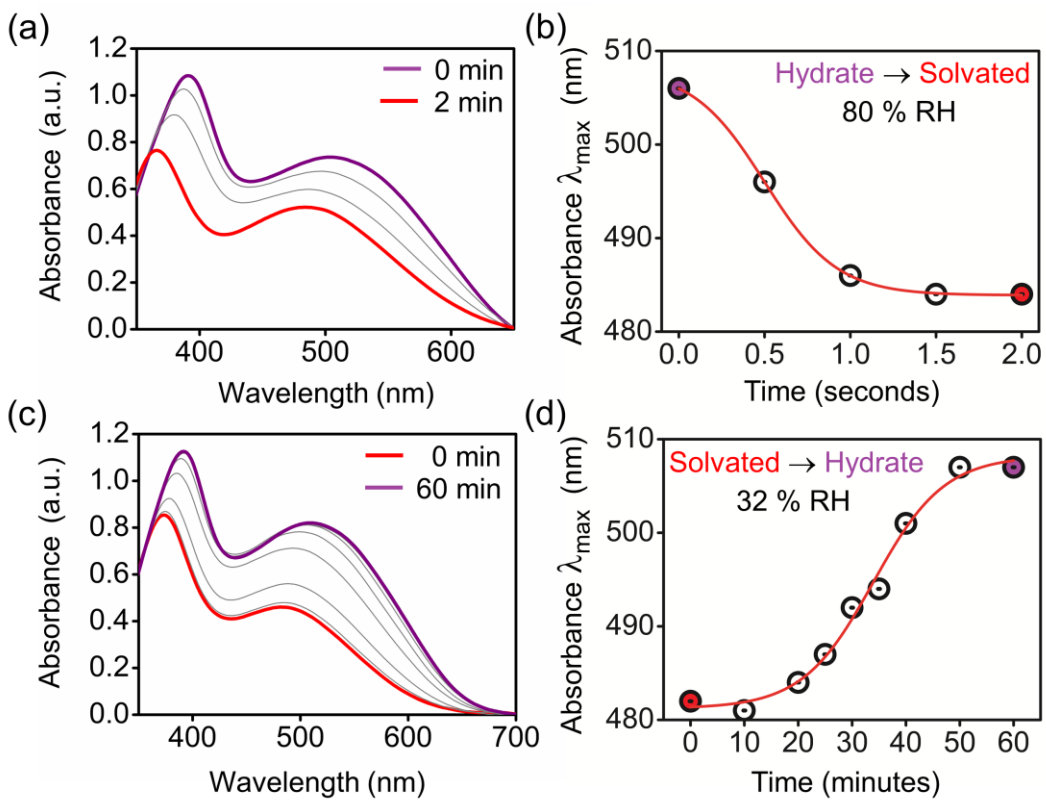

Figure S9: Overlaid absorption spectra and absorption lambda max values (λ_{max}) of a dropcast film of **1**·2Br measured at different time intervals during the conversion of the (a-b) hydrate state (purple trace) to the solvated state (red trace) within an humidity chamber maintained at 80% relative humidity and during the conversion of the (c-d) solvated state to the hydrate state within a humidity chamber maintained at 32% relative humidity.

5. Optical Band Gap Determination

Film reflectometry was employed to measure the thickness of the films of **1**·2Br in all three of its hydration states: as the anhydrate (film thickness = 8.7 μm), the hydrate (film thickness = 8.7 μm), and solvated state (film thickness = 9.1 μm). This thickness allows us to calculate the film absorption coefficient by using a simple Beer-Lambert relation α = 2.303A/t where A is absorbance and t is thickness of the film. Tauc plots based on absorption where then used to calculate the optical band gaps of the xerogel films of **1**·2Br in all three of its hydration states: as the anhydrate (band gap = 2.87 eV), the hydrate (film thickness = 1.97 eV), and solvated state (film thickness = 2.17 eV).

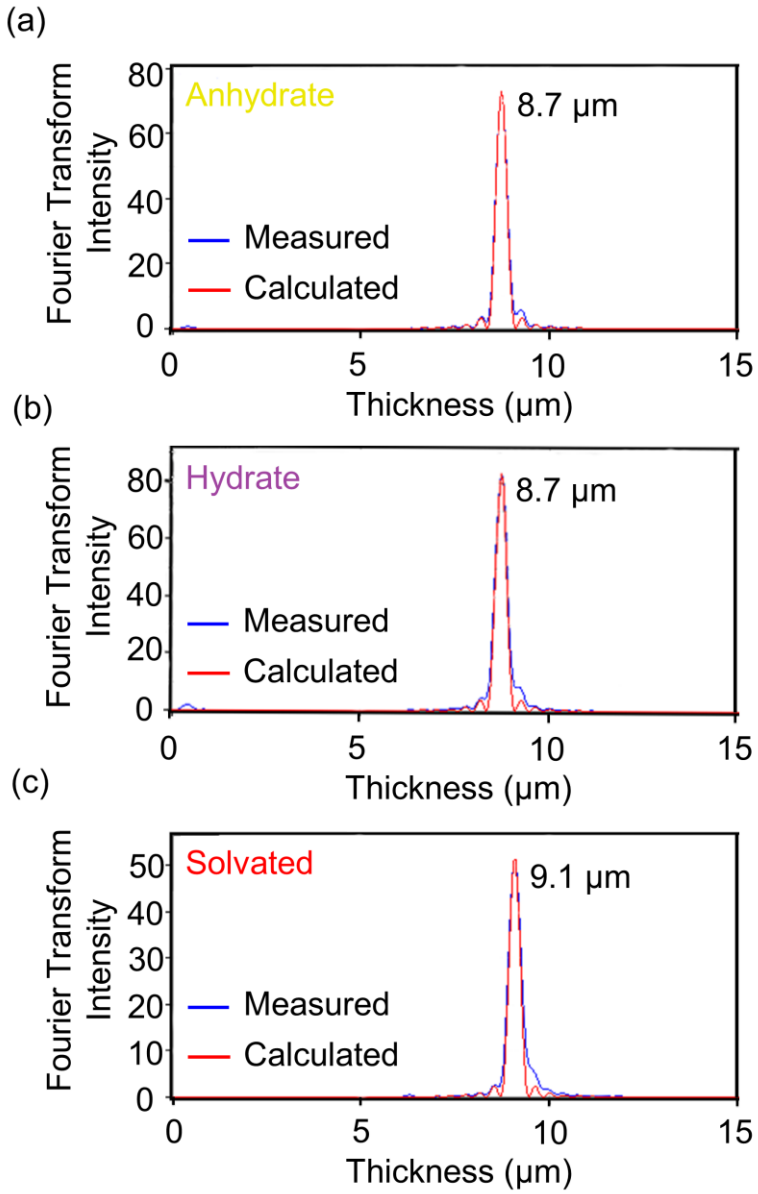

Figure S10: Film thickness histograms of a xerogel film of **1**·2Br in its (a) anhydrated, (b) hydrated, and (c) solvated states determined by film reflectometry.

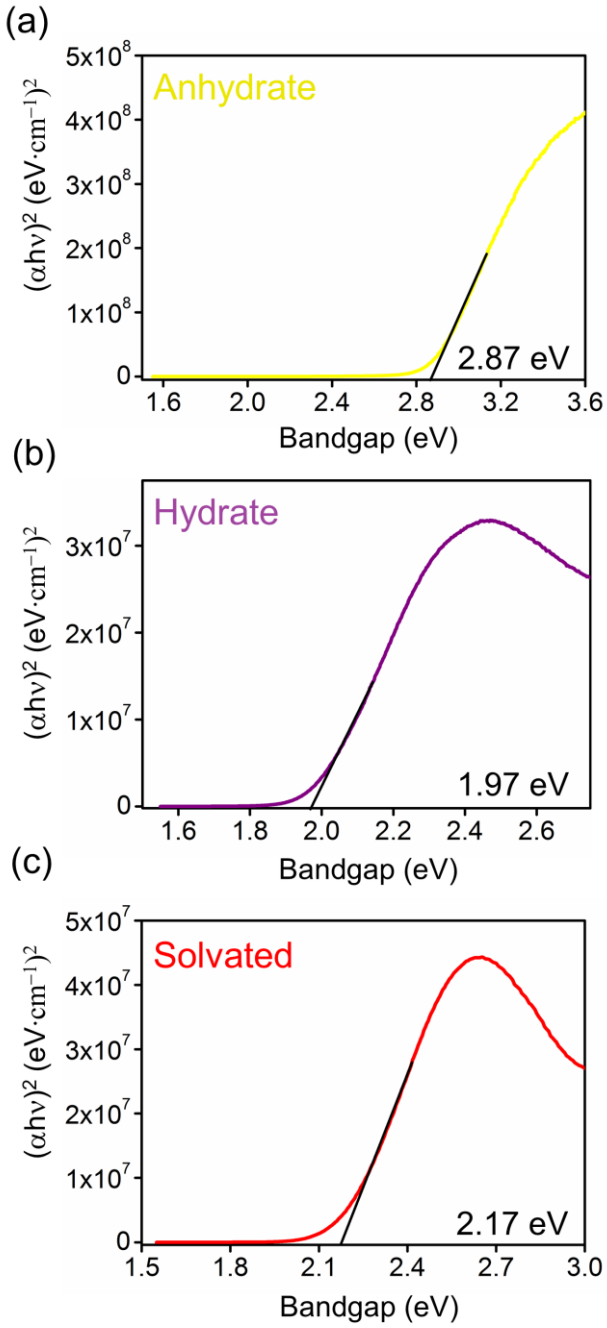

Figure S11: Tauc plots of a film of **1**·2Br in its (a) anhydrated, (b) hydrated, and (c) solvated states.

6. Powder X-ray Diffraction (PXRD)

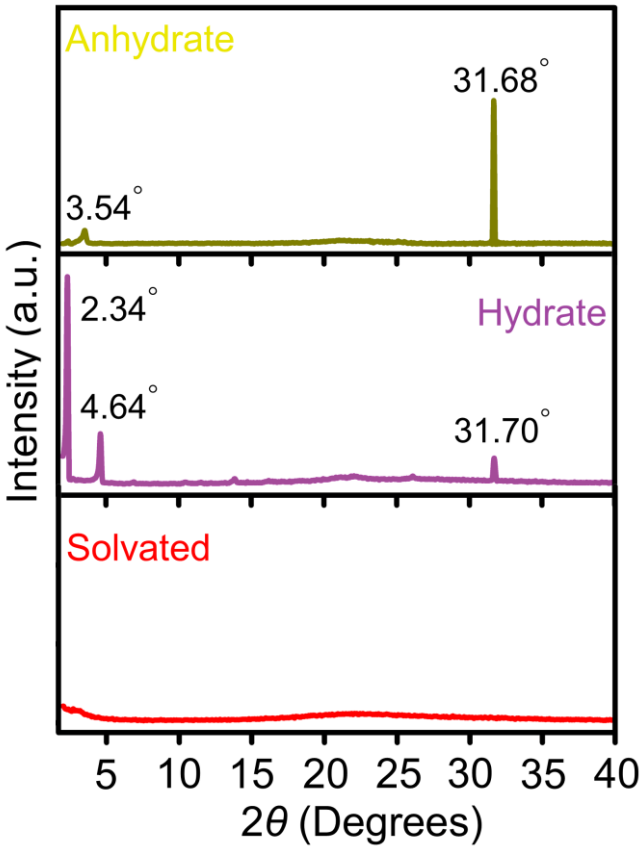

Figure S12: Stacked PXRD patterns of **1**·2Br in its yellow anhydrate state (top), purple hydrate state (middle), and red solvated state (bottom).

7. Dynamic Vapor Sorption (DVS)

Table S2: Pseudo Second Order Rate Constants and Goodness of Fit Values for the Dynamic Water Vapor Adsorption and Desorption of **1**·2Br from 10-90 % Relative Humidity[a]

Relative Humidity[b] (%)	Pseudo Second Order Rate Constant	
	K_2[c] ($g \cdot mg^{-1} \cdot min^{-1}$)	R^2
10 (ads)	4.1×10^{-2}	0.98
10 (des)	9.8×10^{-3}	0.99
20 (ads)	5.1×10^{-2}	0.99
20 (des)	7.4×10^{-3}	0.99
30 (ads)	1.3×10^{-1}	0.99
30 (des)	1.9×10^{-3}	0.99
40 (ads)	9.9×10^{-2}	0.99
40 (des)	1.4×10^{-5}	0.93
50 (ads)	9.1×10^{-2}	0.99
50 (des)	8.0×10^{-3}	0.99
60 (ads)	6.1×10^{-4}	0.99
60 (des)	3.0×10^{-2}	0.99
70 (ads)	1.0×10^{-4}	0.98
70 (des)	1.2×10^{-2}	0.99
80 (ads)	2.3×10^{-3}	0.97
80 (des)	2.9×10^{-4}	0.91
90 (ads)	5.5×10^{-4}	0.99

[a]data obtained starting from the anhydrate state of 1·2Br at 10 % relative humidity with 10 % step-wise increases in relative humidity and back. [b](ads) indicates dynamic water vapor adsorption; (des) indicates dynamic water vapor desorption. [c]Determined from adsorption/desorption kinetic data fitted to a linear pseudo second order kinetic model.

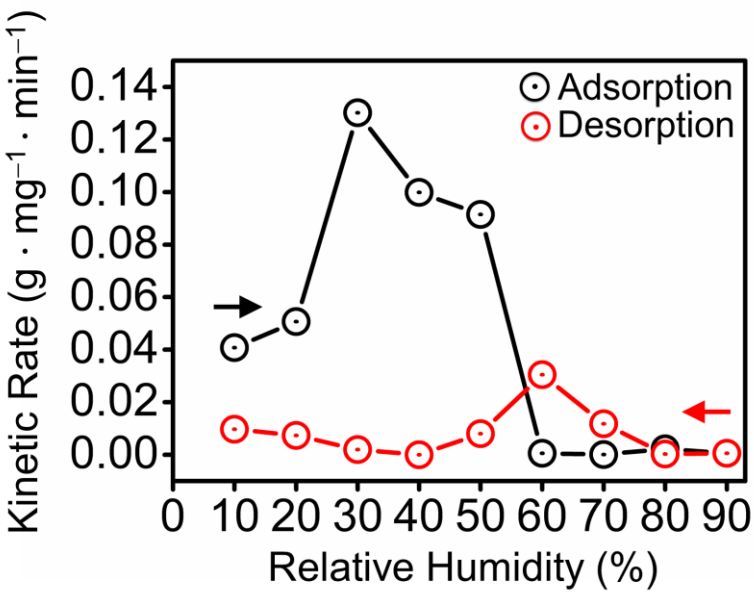

Figure S13: Pseudo second order kinetic rates of dynamic water vapor sorption-desorption versus relative humidity for **1**·2Br cycling from its anhydrate state at 10 % relative humidity to 90 % relative humidity and back.

8. Computational Details

The structural and energetic analysis of the molecular systems described in this study were carried out using the Gaussian09 software.[2] Geometries were optimized in two dielectric to approximate a low water content environment (ε = 5), and water solvation (ε = 78) with DFT[3,4] at the B97-D[5]/Def2-SVP[6,7] level of theory. An ultra-fine integration grid of 99 radial shells and 590 angular points per shell was selected. Stationary points were determined when the maximum gradient convergence tolerance and the root-mean-square gradient were below 0.00045 hartree/Bohr and 0.00030 hartree/Bohr, respectively. Effects of solvent employed the IEF-PCM[8] method in combination with radii and non-electrostatic terms from the SMD[9] solvation model. For more accurate energetics, and charge distribution, single point energy calculations were performed at the B97-D/Def2-QZVP[6,7]//B97-D/Def2-SVP, and B3LYP[10]/Def2-QZVP//B97-D/Def2-SVP, respectively. The rationale for using the aforementioned density functionals resulted from an exhaustive performance study[11] on a broad set of non-covalent interacting systems. In the discussions of the electronic rearrangement upon dimer formation, the total electronic density change caused by the interaction between the donor acceptor system of one self-complex and the donor acceptor

system of the other self-complex is considered and is defined as:

$$\Delta\rho = \rho_{comp.} - \rho_{mono,A} - \rho_{mono,B} \qquad (1)$$

where $\rho_{comp.}$ is the electronic density of the dimer stack and $\rho_{mono,A}$ and $\rho_{mono,B}$ are the electron densities of the individual self-complexes forming the dimer stack in exactly the configuration adopted in the relaxed dimer complex. Within this definition, a positive value indicates electron accumulation and a negative value indicates electron depletion.

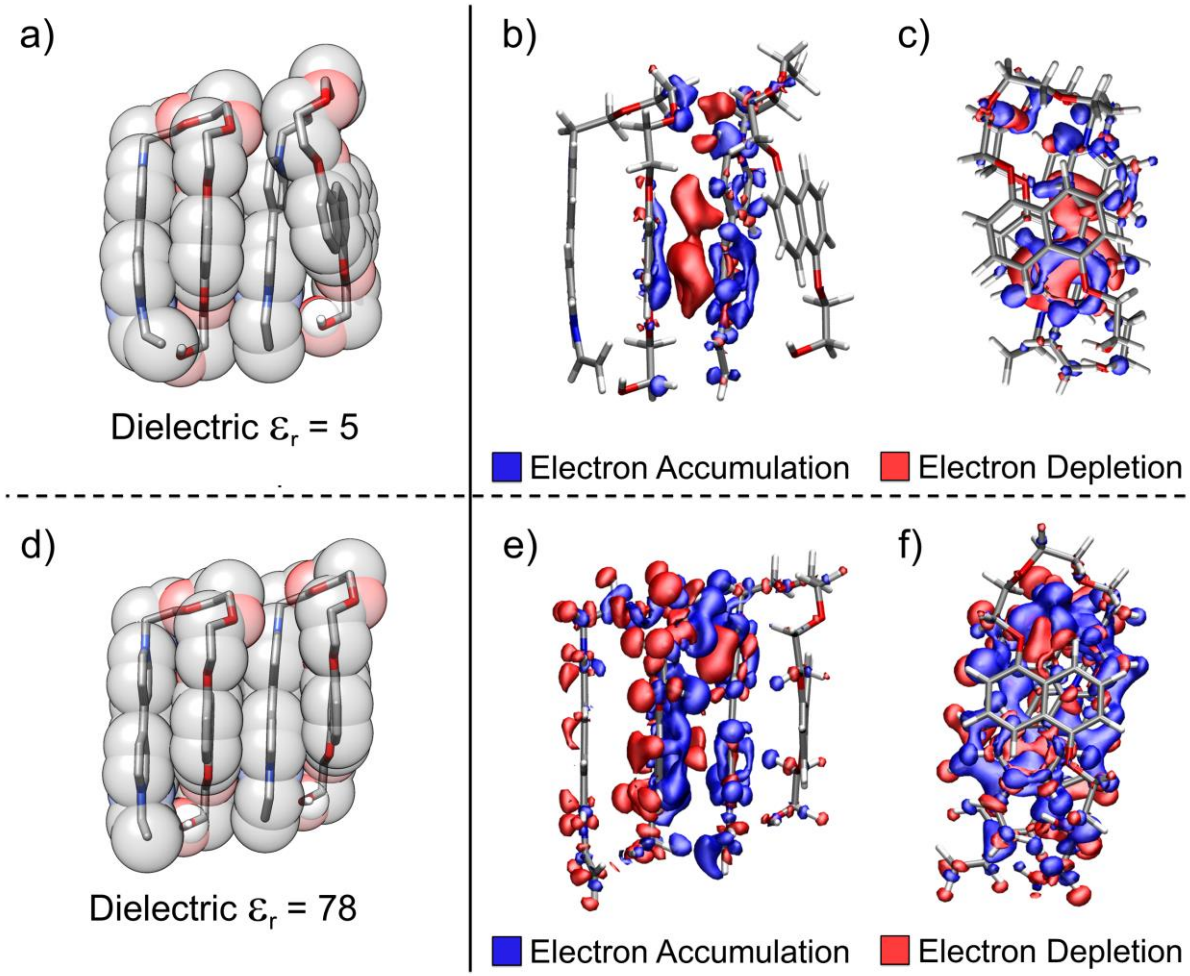

Figure S14: B97-D/Def2-SVP calculated 1 : 1 dimer donor-acceptor complexes of a model self-complex of **1**·2Br, bearing an ethenyl chain, (a,d) and their corresponding total electronic density redistribution upon complexation (b,c,e,f) at dielectric constants of 5 (a-c) and 78 (d-fO). Contours in blue show electron accumulation, and those in red show electron depletion. A contour cutoff value of 0.00025 e− Å−3 was used.

Interaction Energies

Two cases were considered for the interaction energy of the dimer formation. The first interaction takes into account all species in their fully relaxed state, and the interaction energy is referred to as ΔE_{relax}. The second case considers the individual self-complex subunits in the configuration adopted within the dimer, and is referred to as $\Delta E_{restrict}$. In this regard, ΔE_{relax} accounts for the deformation energies upon dimer formation, whereas $\Delta E_{restrict}$ only considers the interactions between the individual self-complexes within the dimer. In both cases, a negative value reflects attraction between the individual self-complex molecules, and a positive values indicates repulsion.

	Low Water Content ($\varepsilon = 5$)	Water-like ($\varepsilon = 78$)
ΔE_{relax}	+9.00	-20.45
$\Delta E_{restrict}$	+7.31	-21.91

Table S3: Interaction energy upon dimerization. Both ΔE_{relax} and $\Delta E_{restrict}$ are computed at the B97-D/Def2-QZVP//B97-D/Def2-SVP level of theory. Energies are reported in [kcal/mol].

References

1. M. A. Olson, J. R. Thompson, T. J. Dawson, C. M. Hernandez, M. S. Messina, T. O'Neal, *Org. Biomol. Chem*., 2013, **11**, 6483.
2. M. Frisch *et al*. Gaussian 09, revision a. 02, gaussian. *Inc., Wallingford, CT* **200,** (2009).
3. P. Hohenber, W. Kohan, *Physical Review*, 1964, **136**, B864.
4. W. Kohn, L. J. Sham, *Physical Review*, 1965, **140**, A1133.
5. S. Grimme, *J. Comput. Chem*., 2006, **27**, 1787.
6. F. Weigen, R. Ahlrichs, *Phys. Chem. Chem. Phys*., 2005, **7**, 3297.
7. F. Weigeng, *Phys. Chem. Chem. Phys*., 2006, **8**, 1057.
8. G. Scalmani, M. J. Frisch, *J. Chem. Phys*., 2010, **132**, 114110.
9. A. V. Marenich, C. J. Cramer, D. G. Truhlar, *J. Phys. Chem. B*., 2009, **113**, 6378.
10. Becke, A. D. Density-functional thermochemistry. III. The role of exact exchange. *J. Chem. Phys.* **98,** 5648–5652 (1993).
11. L. M. Roch, K. K. Baldridge, *J. Chem. Theory Comput*., 2017, **13**, 2650.